ORNL/TM-6949

DE-2931

MASTER

Shielding Calculations for the TFTR Neutral Beam Injectors

R. T. Santoro
R. A. Lillie
R. G. Alsmiller, Jr.
J. M. Barnes

OAK RIDGE NATIONAL LABORATORY
OPERATED BY UNION CARBIDE CORPORATION · FOR THE DEPARTMENT OF ENERGY

ORNL/TM-6949
Dist. Category UC-20d
(Fusion Systems)

Contract No. W-7405-eng-26

Engineering Physics Division

Shielding Calculations for the TFTR Neutral Beam Injectors*

R. T. Santoro
R. A. Lillie
R. G. Alsmiller, Jr.
J. M. Barnes+

*Submitted for
Journal publication

+Computer Sciences Division

Date Published - July 1979

OAK RIDGE NATIONAL LABORATORY
Oak Ridge, Tennessee 37830
operated by
UNION CARBIDE CORPORATION
for the
DEPARTMENT OF ENERGY

ABSTRACT

Two-dimensional discrete ordinates calculations have been performed to determine the location and thickness of concrete shielding around the Tokamak Fusion Test Reactor (TFTR) neutral beam injectors. Two sets of calculations were performed: one to determine the dose equivalent rate on the roof and walls of the test cell building when no injectors are present, and one to determine the contribution to the dose equivalent rate at these locations from radiation streaming through the injection duct. Shielding the side and rear of the neutral beam injector with 0.305 and 0.61 m of concrete, respectively, and lining the inside of the test cell wall with an additional layer of concrete having a thickness of 0.305 m and a height above the axis of deuteron injection of 3.10 m is sufficient to maintain the biological dose equivalent rate outside the test cell to $\sim$ 1 mrem/DT pulse.

INTRODUCTION

The D-T fusion reactions in the Tokamak Fusion Test Reactor (TFTR)* will be initiated by the injection of neutral deuterium into a magnetically confined tritium plasma. The deuterons heat the plasma via collisions with the tritium and also react with the tritium to produce $\sim$ 14 MeV neutrons in D-T reactions. The deuterons are energized and then neutralized in neutral beam injectors[1] and directed into the reactor through ducts that extend from the injectors and pass through a concrete, pillbox-shaped (igloo) shield that surrounds the reactor.

The reactor, igloo, and the neutral beam injectors are housed in a large, concrete building referred to as the test cell. The thickness of the concrete forming the igloo and the test cell is sufficient to reduce the biological dose equivalent rate outside of the test cell to an acceptable limit of $\sim$ 1 mrem/D-T pulse when no injectors are present. However, neutrons and gamma rays also stream through the injection ducts resulting in an increase in the dose rate outside both the walls and roof of the test cell. In this paper, the results of two-dimensional neutronics calculations to determine the location and thickness of additional concrete shielding around the neutral beam injectors necessary for reducing the dose rate due to neutron streaming are reported.

In a previous paper[2], the results of two- and three-dimensional neutronics calculations to determine the nuclear heating rates and neutron and gamma ray scalar flux distributions in vital components inside the neutral beam injectors were presented. This work is an extension of that

---

*Under construction at the Princeton Plasma Physics Laboratory.

described in Ref. 2 and incorporates many of the same calculational procedures and models. Also, the spatial distributions of the neutron flux in the calculational models in this study were used as input data to a companion analysis reported by Alsmiller et al.,[3] to estimate the biological dose equivalent rates in the test cell from neutron induced activation.

The calculation models and methods are described in Section II and the results are presented and discussed in Section III.

DETAILS OF THE CALCULATIONS

The calculations to estimate the biological dose rates outside the test cell were carried out using two-dimensional radiation transport methods in two separate calculational sequences. In the first, only the reactor, igloo, and test cell were modeled in order to determine the dose rates when no injectors are present. In the second, an injector and the test cell were modeled to obtain the contributions to the dose rate outside the test cell from radiation streaming through the injection duct.

The reactor, igloo, and test cell were represented in r-z geometry with toroidal symmetry about the z-axis using 65 axial and 76 radial mesh intervals. A schematic representation of the geometry is shown in Fig. 1. Some of the poloidal magnetic field coils are included in the model, but the toroidal field coils were omitted since it is not possible to account for the finite toroidal extent of these coils in this two-dimensional geometry. Omitting the toroidal field coils leads to conservative estimates of the biological dose rates since the shielding effects of the coils are not taken into account.

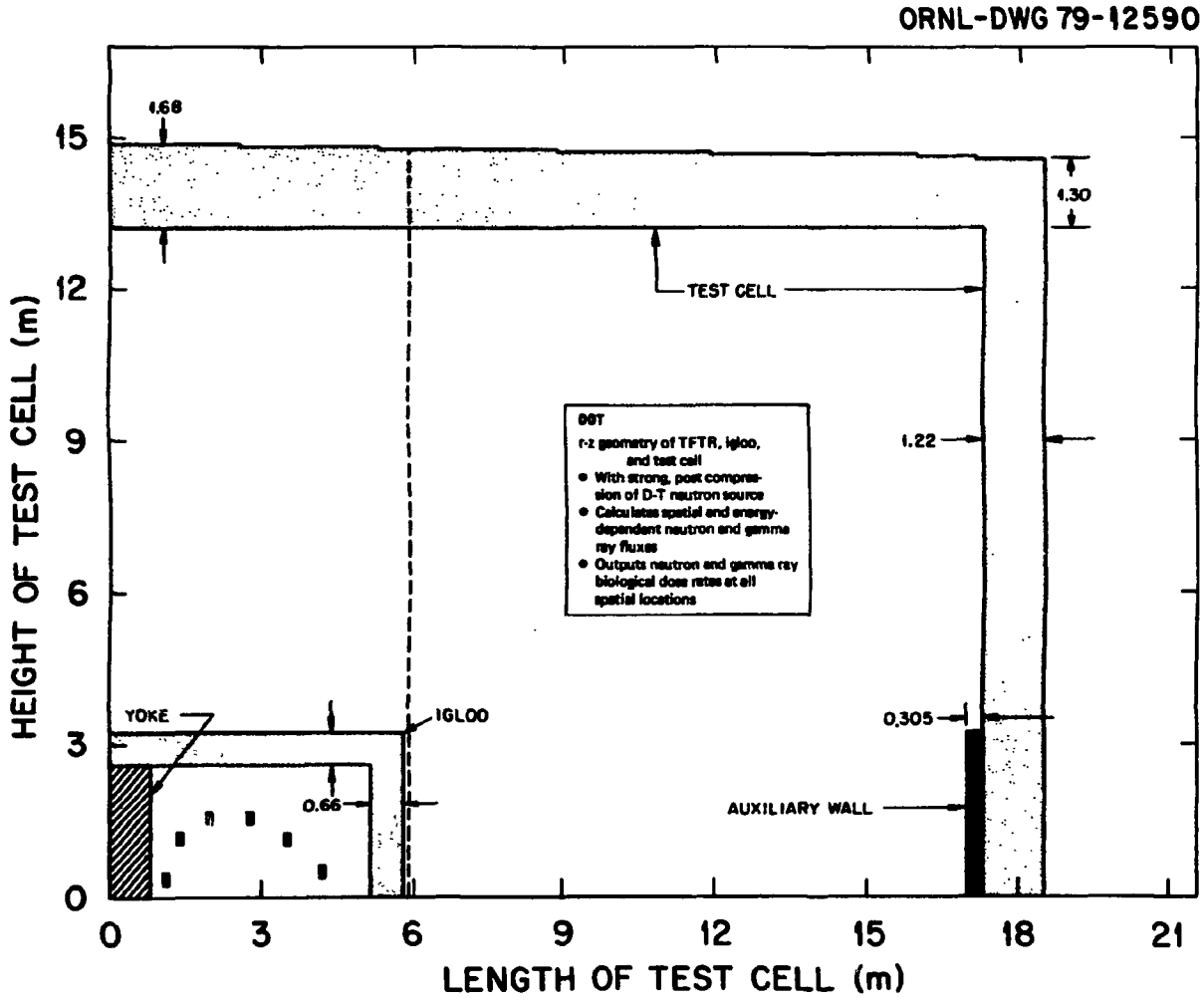

Fig. 1. Two-dimensional calculations model of the test cell and igloo.

The walls and roof of the igloo are concrete having a uniform thickness of 0.66 m. The yoke is stainless steel type 316 having a reduced density of 0.25 ρ_{SS} to account for the tubular construction of the actual yoke. The test cell roof is 1.68 m thick at the center and tapers uniformly to a thickness of 1.30 m at the wall. The taper in the roof was approximated using seven step changes in the roof thickness. The inner surfaces of the test cell are coated with borated plaster having a thickness of 0.01 m. The walls have a uniform thickness of 1.22 m. Also shown in a 0.305-m thick auxiliary wall on the inside of the test cell wall. This was added to provide additional shielding for the energetic neutrons that stream through the injection ducts.

The calculation of the dose equivalent rate was accomplished using a neutron source corresponding to that at strong, postcompression of the plasma.[4] It is anticipated that the neutron yield will be greatest under these conditions. It should also be noted that the r-z geometry used here accounts for the toroidal extent of the neutron distribution. The neutron transport, as indicated in the inset in Fig. 1, was carried out using the two-dimensional discrete ordinates code DOT.[5] The neutron and secondary gamma ray flux were calculated as a function of energy at all spatial locations and stored on magnetic tape for subsequent analysis.[3] These data were also folded with flux-to-biological dose equivalent rate conversion factors to yield the spatial distributions of the dose rate. This calculation, as noted above, estimates the dose outside the test cell when no penetration exists in the igloo and is, to some extent, the lower limit of the dose rate during operation of the reactor.

The model of an injector and the test cell used in the second calculation is shown in Fig. 2. In this representation, the injector axis is normal to the plasma axis. In the TFTR, neutral particles are injected into the plasma approximately tangent to the plasma axis. The calculatonal sequence described below to determine the radiation source incident on the injector takes into account tangential injection. These components, as well as those comprising the injector, were represented using 143 axial and 61 radial mesh intervals but with symmetry about the axis of injection. The portion of the test cell shown in Fig. 2 corresponds to that to the right of the igloo indicated by the dashed line in Fig. 1. The injector and its components were modeled in the same detail as in the two-dimensional analysis discussed in Ref. 2. The injector is shown with 0.305 m of concrete shielding around the lateral surface and with 0.61 m on the rear surface. Calculations were performed with and without this shielding present.

The calculations to estimate the dose equivalent rate using this geometry are more complex than those employed for the geometry in Fig. 1. The calculational procedure, shown in Fig. 3, also involves two sequences; one to define the radiation source and one to transport the radiation through the injector and test cell. The procedures are essentially the same as those described in Ref. 2 so only the salient features will be discussed here.

In the source preparation, the energy, spatial, and angular distributions of the neutrons and gamma rays that stream through the injector duct and leak through the igloo wall were obtained. An initial calculation was performed using the DOT code to define an interior boundary source

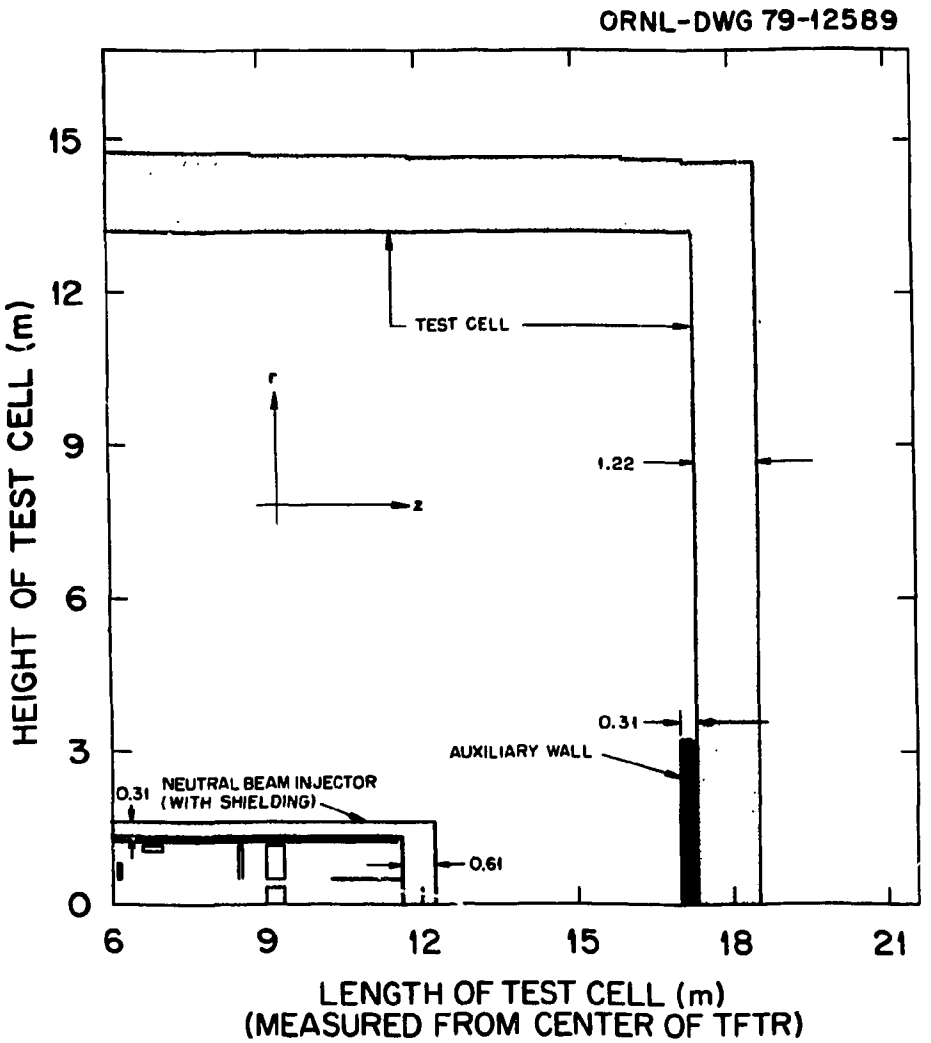

Fig. 2. Two-dimensional calculational model of the test cell and the neutral beam injector.

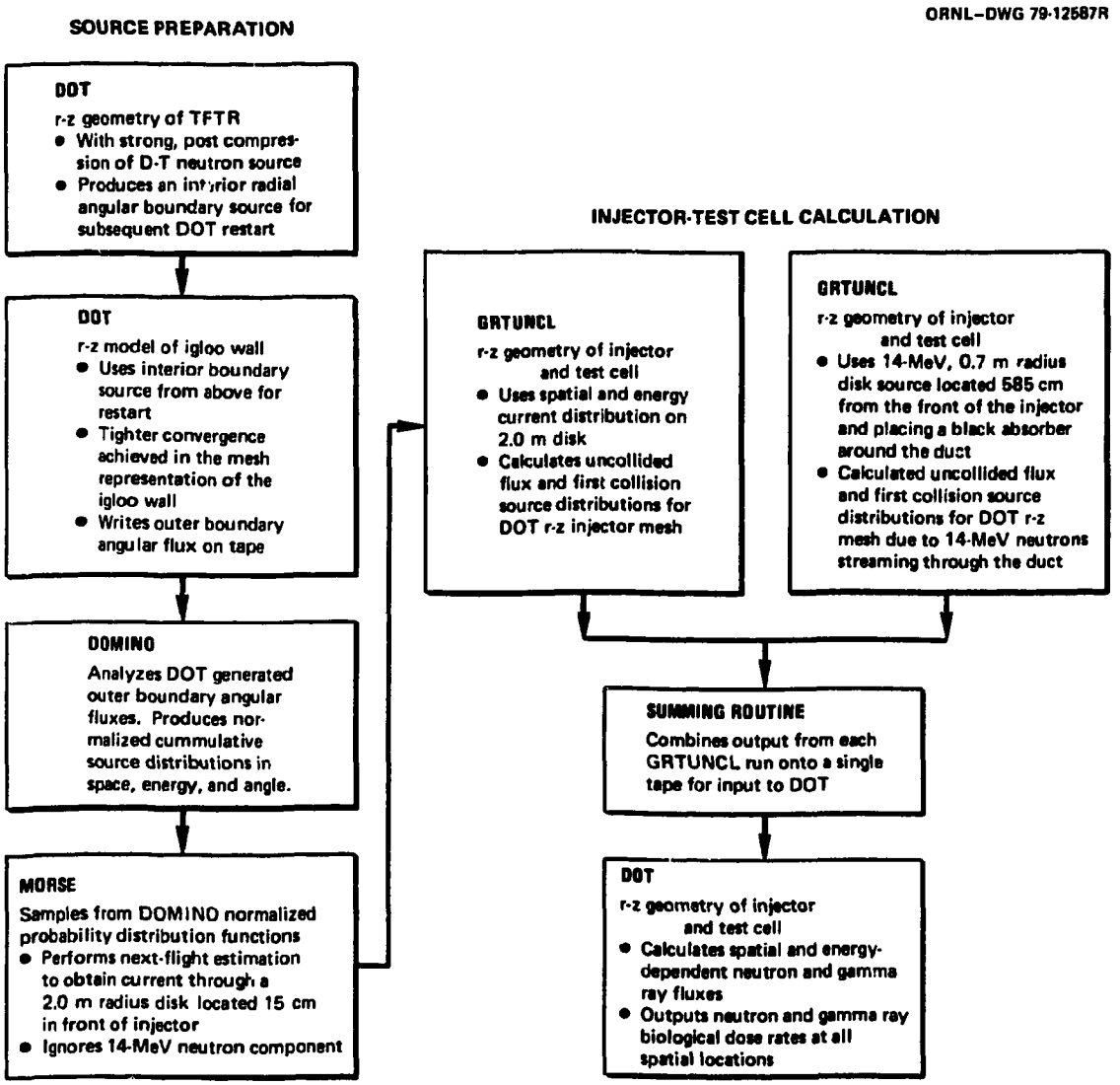

Fig. 3. Calculational sequences used to estimate the contributions to the dose equivalent rate on the test cell roof and walls due to streaming through the neutral beam injector.

term inside the igloo using the reactor-igloo model shown in Fig. 4. The components were modeled in r-z geometry with toroidal symmetry about the z-axis using 61 radial and 38 axial mesh intervals to describe the geometry. The neutron source was taken to be that at strong, postcompression of the plasma. An interior boundary source was obtained at the location shown in Fig. 4. This source includes the neutrons emitted from the plasma as well as neutrons and gamma rays resulting from primary neutron reactions in the yoke, igloo, and poloidal coils.

The interior boundary source was used as the input to a second DOT calculation to obtain the angular flux at the radial boundary of the igloo. For this calculation, the igloo was represented in r-z geometry using 26 radial and 38 axial mesh intervals with symmetry about the toroidal axis of the TFTR. In this reduced geometry, a tighter convergence of the flux is obtained in the finer mesh representation of the igloo wall. Two separate calculations were performed using the reduced geometry to obtain the boundary flux "with" and "without" the injector duct in the igloo wall. For the case "with" the 0.42-m high injector duct, the 0.42-m high cross-hatched portion of the igloo wall shown in Fig. 4 was treated as a void. In a two-dimensional geometry, the duct opening extends completely about the torus. The finite toroidal extent of the duct opening was accounted for in the preparation of the disc source used as the input to the injector-test cell analysis.

The boundary angular flux data for the cases "with" and "without" the injector penetration were then each processed using the DOT-to-MORSE coupling code DOMINO.[6] This code produces cumulative distributions in energy, space and polar and azimuthal angles for subsequent source input

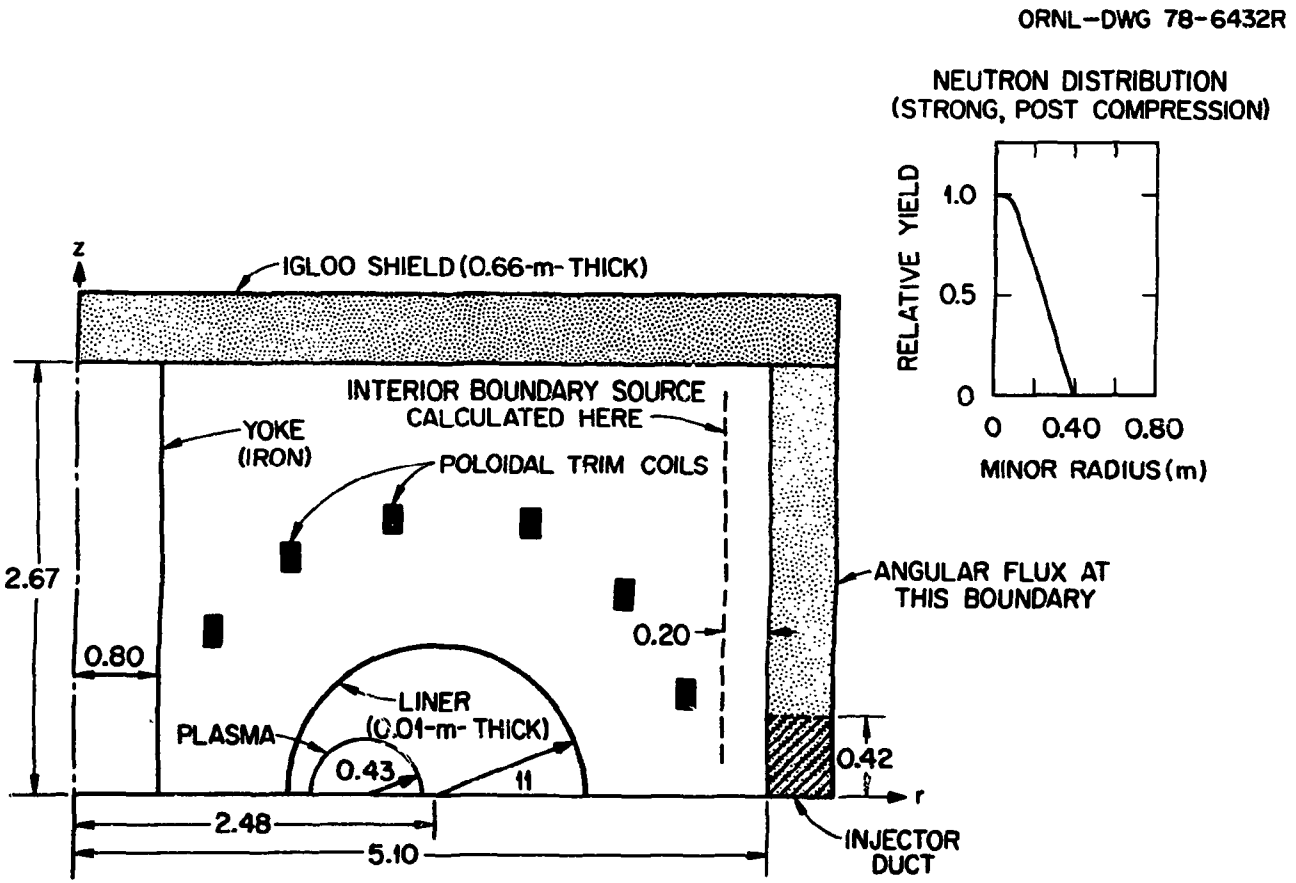

Fig. 4. Two-dimensional calculational model of the TFTR and the igloo used to obtain the energy, spatial, and angular distributions of neutrons and gamma rays incident on the injector.

to the MORSE code.[7] The boundary flux data for the case "with" the injector penetration was processed for all but the 14-MeV neutron group which corresponds to the energy of those neutrons which stream directly through the injector duct opening in the igloo. These neutrons are not properly accounted for in the DOT boundary angular flux data because the S_8 quadrature used in the DOT toroidal calculations does not contain angular directions that permit streaming along the radial axis. While this can be remedied using a highly biased and consequently large tailored quadrature set, the computational time for the toroidal calculations would be prohibitively long. All energy groups were processed for the case "without" the injector penetration.

The radiation source which accounted for all but the 14-MeV neutron streaming used as the input to the injector-test cell analysis was obtained by calculating the radially-varying multigroup current through a 2.0-m radius disc located 0.15 m in front of the injector housing. The disc was divided into 20 radial and 10 azimuthal intervals centered about the axis of injection and the current was calculated using the point detector estimator in the MORSE code. The normalized cumulative distributions from DOMINO for the configurations "with" and "without" the duct penetration served as the input to the disc source preparation. The radial variation and total source strength were obtained by summing the contributions to the current over the azimuthal intervals and correcting for the anisotropy of the DOMINO source, respectively. For the case "without" the duct present, the radiation source is comprised of neutrons and secondary gamma rays that leak through the igloo wall. For the case "with" the duct present, the contribution to the source term from radiation

scattered through the opening from inside the igloo is accounted for.

The 14-MeV neutrons streaming through the injector port, which were not included in the disc source data, were accounted for in a separate calculation. In this calculation, a 0.7 m radius isotropic 14-MeV neutron source disc was placed at the intersection of the axis of injection and the plasma toroidal axis. This location, which corresponds to a distance of 5.85 m from the front of the injector housing, was chosen such that the disc source represented the plasma volume viewed through the duct opening by the injector. To ensure that neutrons emitted from this source passed only through the duct opening, a black absorber was used to define the duct opening.

The uncollided flux and first collision source in the injector and test cell for both the 2.0 and 0.7 m radius disc sources were then obtained using GRTUNCL.[8] This code calculates the uncollided flux and the first collision source at each mesh interval in the geometry in Fig. 2 and records these data on magnetic tape for subsequent use in DOT. The advantage of employing GRTUNCL is the elimination of ray effects. The uncollided flux and first collision source data obtained from the two GRTUNCL calculations were appropriately normalized and summed over all mesh intervals and used as the input to the DOT code.

The DOT code completes the radiation transport and combines the collided flux distribution with the uncollided flux from the GRTUNCL calculations. The DOT code outputs the spatial distributions of the biological dose rate and also writes the spatial and energy distributions of the neutron and gamma ray flux on magnetic tape.

All of the discrete ordinates calculations were performed using an S_8 angular quadrature. The radiation transport was accomplished using a 35 neutron, 21 gamma ray energy group transport library obtained by collapsing the 171-neutron 36-gamma ray energy group VITAMIN C (ENDF/B-IV) data set.[9] In all cases, the scattering cross sections were represented with a P_3 Legendre expansion. The neutron fluxes were converted to dose equivalent rates using flux-to-dose equivalent conversion factors suggested by the NCRP[10] and the gamma ray flux-to-dose conversion factors were taken from Claiborne and Trubey.[11]

The compositions of the materials used in the calculations are given in Table I. The concrete used in the igloo and to shield the neutral beam injector and the concrete used in the auxiliary wall each contain boron and barium and are effective mixtures for shielding against neutrons. The test cell concrete is more typical of that used in construction. The charged deuteron bending magnet in the neutral beam injector is composed of iron[2] and the injector calorimeter and TFTR poloidal field coils are composed of copper. The magnet yoke and injector structure are stainless steel type 316.

III. DISCUSSION OF RESULTS

The biological dose rate as a function of distance along the test cell roof is shown in Fig. 5. The curve labeled "without injector" shows the dose rate obtained using the reactor, igloo, and test cell calculational model in Fig. 1. The curves labeled "shielded injector" and "unshielded injector" show the contributions to the dose rate on the roof from radiation streaming through the neutral beam injector. These data were obtained using the calculational model in Fig. 2 and correspond to

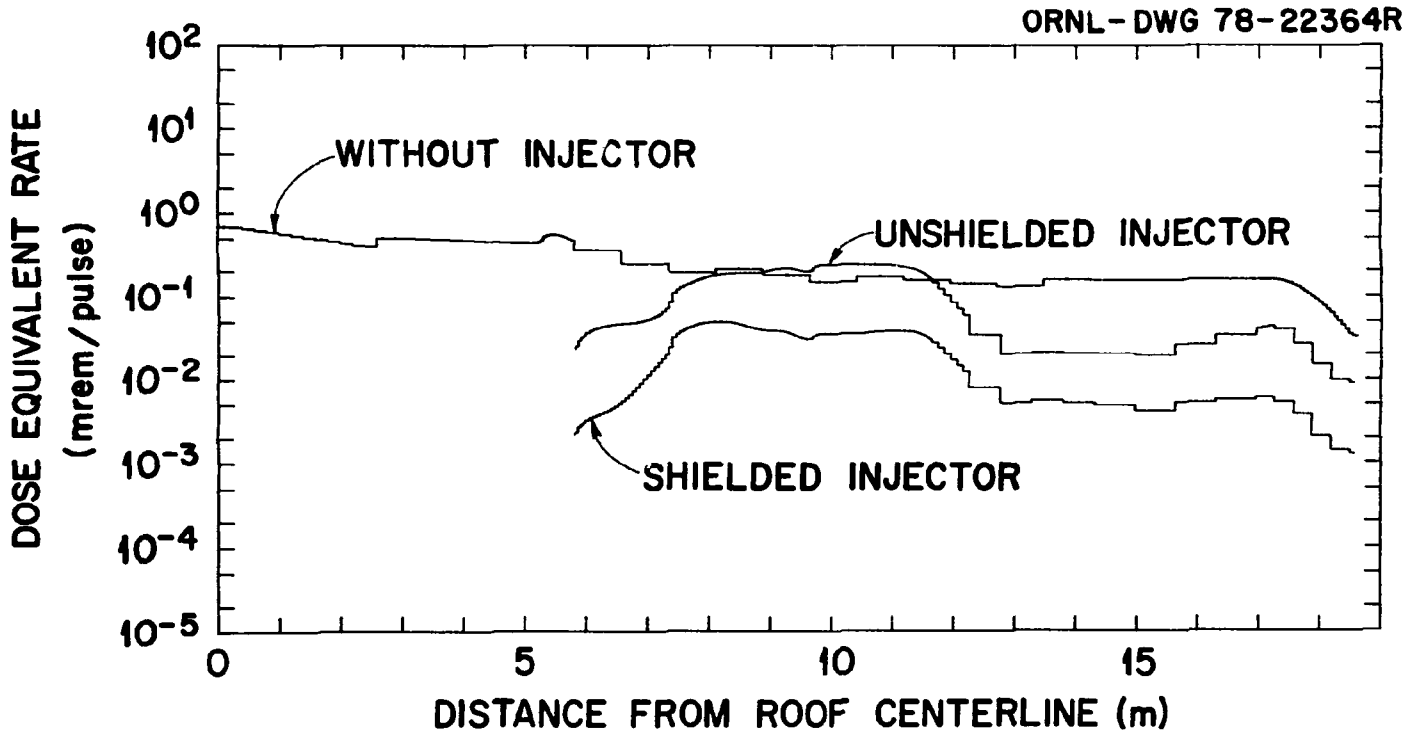

Fig. 5. Dose equivalent rate as a function of distance from the roof centerline.

Table I

COMPOSITION OF MATERIALS USED IN THE CALCULATIONS

Element	Composition (Atoms/cm•Barn) Igloo and Injector Shield Concrete	Auxiliary Wall Concrete	Test Cell Concrete	Borated Plaster	Iron	Copper	SS-316*
H	$8.246 \cdot 10^{-3}$	$7.830 \cdot 10^{-3}$	$7.830 \cdot 10^{-3}$	$2.43 \cdot 10^{-2}$			
B	$1.097 \cdot 10^{-3}$	$1.058 \cdot 10^{-3}$		$3.77 \cdot 10^{-1}$			
C	$1.052 \cdot 10^{-2}$						$1.99 \cdot 10^{-4}$
D	$4.322 \cdot 10^{-2}$	$4.396 \cdot 10^{-2}$	$4.385 \cdot 10^{-2}$	$3.15 \cdot 10^{-2}$			
Na	$1.310 \cdot 10^{-5}$	$9.955 \cdot 10^{-4}$	$1.048 \cdot 10^{-4}$				
Mg	$1.822 \cdot 10^{-4}$	$1.486 \cdot 10^{-4}$	$1.486 \cdot 10^{-4}$				
Al	$2.634 \cdot 10^{-4}$	$2.366 \cdot 10^{-3}$	$2.389 \cdot 10^{-3}$				
Si	$1.091 \cdot 10^{-3}$	$1.507 \cdot 10^{-2}$	$1.580 \cdot 10^{-2}$				$1.36 \cdot 10^{-3}$
S	$8.077 \cdot 10^{-5}$	$5.635 \cdot 10^{-5}$	$5.635 \cdot 10^{-5}$	$3.37 \cdot 10^{-3}$			
K	$1.386 \cdot 10^{-5}$	$6.778 \cdot 10^{-4}$	$6.932 \cdot 10^{-4}$				
Ca	$1.308 \cdot 10^{-2}$	$2.975 \cdot 10^{-3}$	$2.915 \cdot 10^{-3}$	$3.38 \cdot 10^{-3}$			
Cr							$1.15 \cdot 10^{-2}$
Mn							$1.65 \cdot 10^{-2}$
Fe	$1.499 \cdot 10^{-4}$	$2.912 \cdot 10^{-4}$	$3.127 \cdot 10^{-4}$		$8.48 \cdot 10^{-2}$		$5.43 \cdot 10^{-2}$
Ni							$1.06 \cdot 10^{-2}$
Cu						$8.48 \cdot 10^{-2}$	
Mo							$1.29 \cdot 10^{-3}$
Ba	$1.245 \cdot 10^{-4}$	$1.184 \cdot 10^{-4}$					

*The composition of the magnet yoke was taken to have a density of 0.25 ρ_{SS-316}

the cases when the concrete shielding about the injector is included and excluded. These data, as well as those presented below, are normalized to a neutron yield of 7×10^{18} n/s during a D-T pulse of 0.5 s duration.

The dose equivalent rate without the injector present has a maximum value of $\sim$ 0.7 mrem/pulse at the center of the roof and decreases to a fairly constant value of $\sim$ 0.2 mrem/pulse at distances along the roof greater than 6 m from the center. The contribution to the dose rate on the roof from radiation streaming and scattering in an unshielded neutral beam injector is $\sim$ 0.3 mrem/pulse between about 8 and 11 m from the roof centerline and at distances beyond 13 m the dose rate is about an order of magnitude smaller. Covering the sides and rear of the injector with 0.305 and 0.61 m of concrete shielding, respectively, reduces the dose rate by nearly an order of magnitude compared to that for an unshielded injector.

The TFTR is designed to operate with four neutral beam injectors all located on the same side of the reactor. Consequently, the dose equivalent rate on the roof above the neutral beam injector cluster is the sum of the dose rate without the injector plus approximately four times the contribution to the dose rate from the shielded or unshielded injector. If the injectors are not shielded, the total dose rate on the roof above the injectors is $\sim$ 1.4 mrem/pulse which is an upper limit of the dose rate. These results do not take into account the shielding of one injector by the adjacent injector(s) and the dose rate at all locations on the roof is taken to be the same as that above one injector when its contribution to the dose rate is increased by a factor of four. Shielding the injectors reduces the total dose rate to $\sim$ 0.32 mrem/pulse. The dose rate along

the roof on the side opposite of where the neutral beam injectors are located will be very nearly the same as that shown by the curve without the injectors present.

The dose rate on the outside of the test cell wall as a function of distance above the injector centerline is shown in Fig. 6. The curves have the same meaning as above. In this case, the dose rate without the injector present has a peak value of $\sim$ 3.5 mrem/pulse at a height of approximately 4 m above the injector axis and an average value of 2 mrem/pulse between 4 and 10 m. The auxiliary shield wall provides sufficient additional shielding to reduce the dose rate to < 1 mrem/pulse at distances above the beam centerline between 0 and 3 m.

For the unshielded injector, the dose rate outside the wall peaks between 0- to 1.5 m as the result of 14 MeV neutrons that stream directly from the plasma region through the injection duct and the injector. At all other locations on the wall, the contribution to the dose rate from radiation leaking through the unshielded injector is small compared to the dose rate when the injector is not present. The addition of 0.61 m of concrete on the back of the injector reduces the dose rate from neutron streaming by nearly three orders of magnitude. Placing 0.305 m of concrete around the sides of the neutral beam injector reduces the dose rate compared to that for an unshielded injector by about an order of magnitude at distances above the beam centerline greater than 3 m.

The biological dose rate as a function of distance along the igloo roof and walls is shown in Fig. 7. The dose rates as a function of distance along the sides and rear of the neutral beam injector for the cases when the injector is shielded and unshielded are shown in Figs. 8

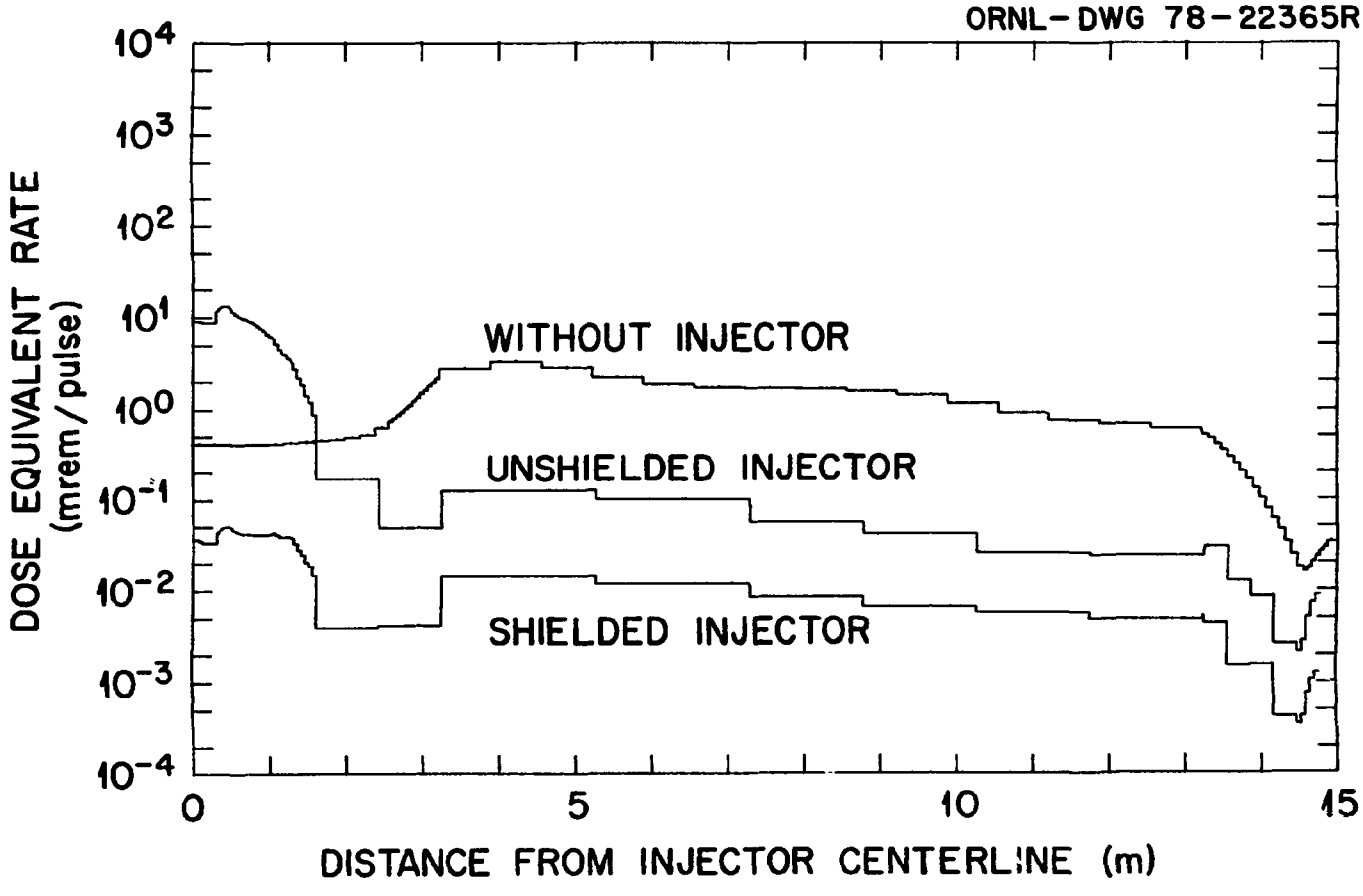

Fig. 6. Dose equivalent rate outside the test cell wall as a function of distance from the injector centerline.

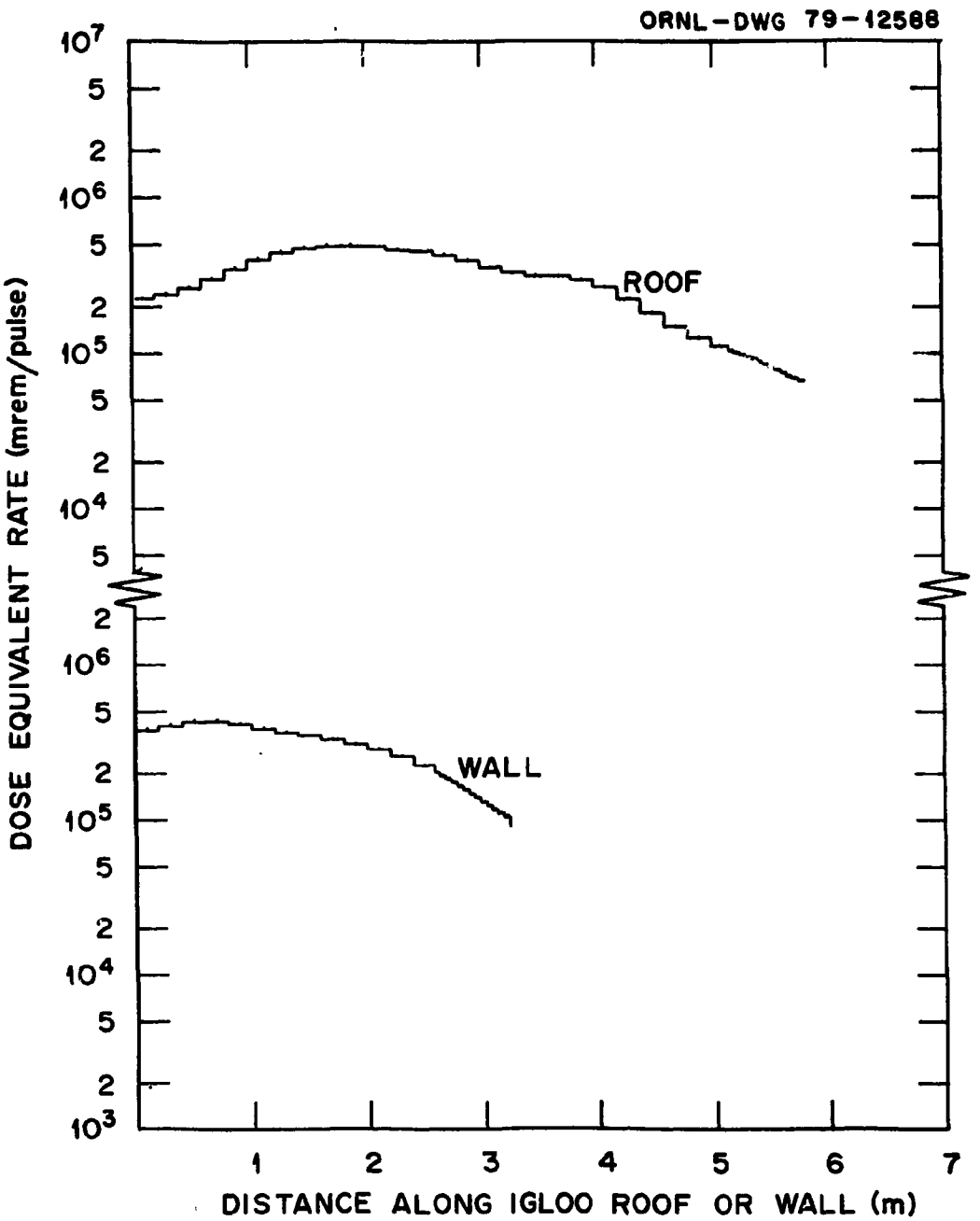

Fig. 7. Dose equivalent rate as a function of distance along the roof and wall of the igloo.

and 9, respectively. The important point to infer from these data is the severe radiation environment inside the test cell during operation of the TFTR. Also, the effectiveness of the shielding around the neutral beam injector as seen in Figs. 8 and 9.

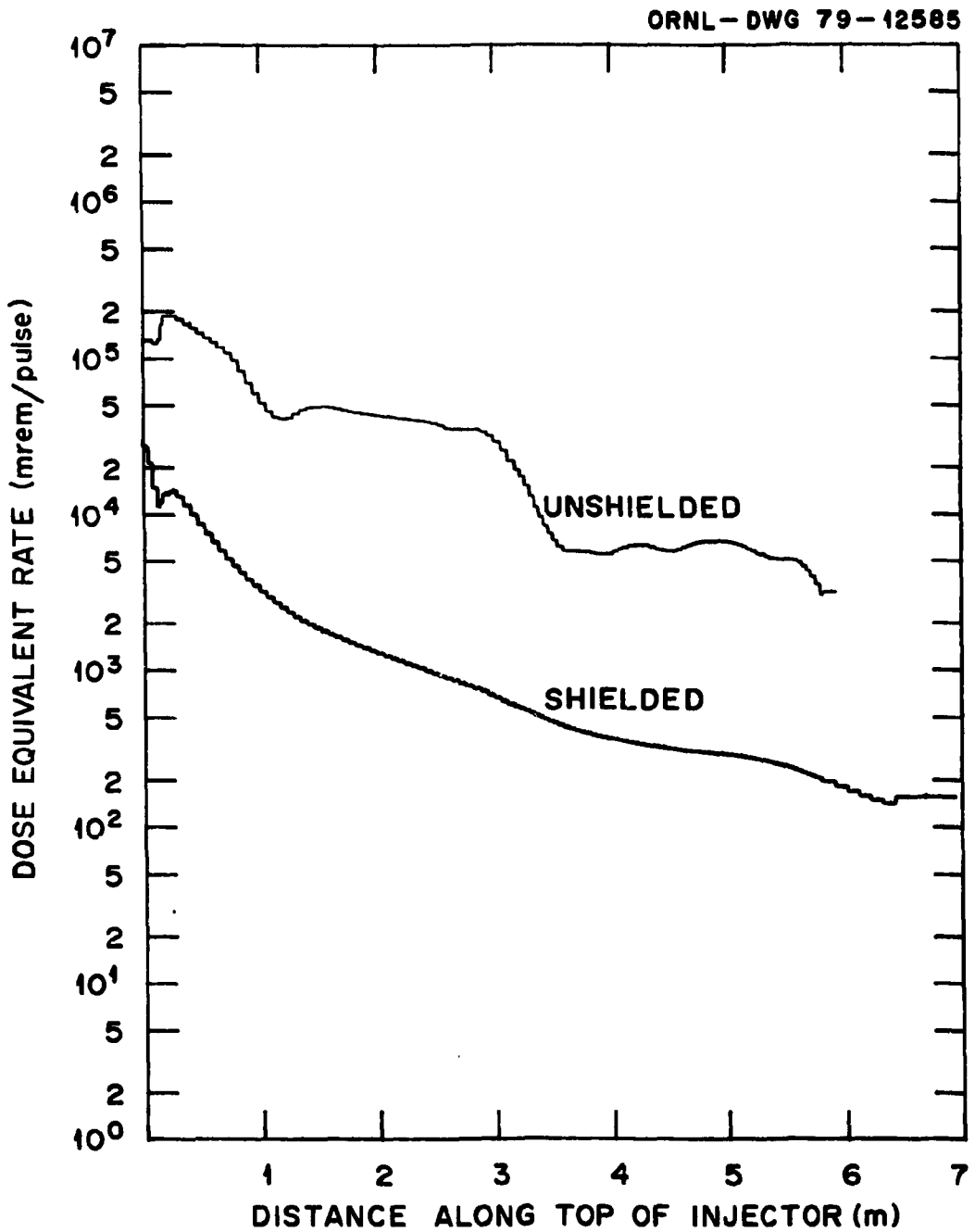

Fig. 8. Dose equivalent rate as a function of distance along the neutral beam injector.

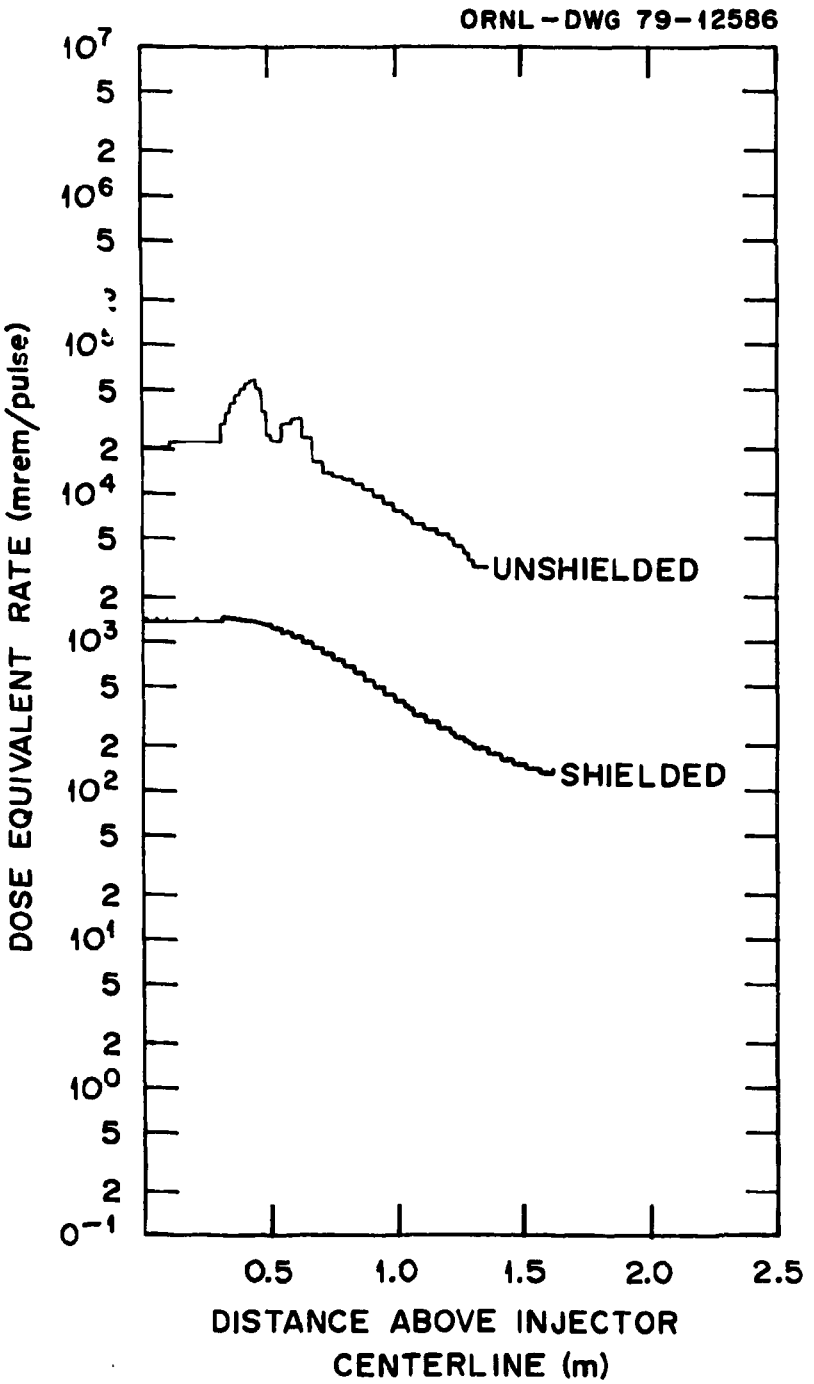

Fig. 9. Dose equivalent rate along the rear of the neutral beam injector as a function of distance above the injector centerline.

References

1. L. C. Pittenger, R. R. Stone, L. E. Valby and L. R. Pedrotti, "A Neutral Beam Injection System for the Tokamak Fusion Test Reactor," Proceedings of the Seventh Symposium on Engineering Problems of Fusion Research, Knoxville, TN, October 25-28, 1977, Vol. I, pp. 555-559.
2. R. T. Santoro, R. A. Lillie, R. G. Alsmiller, Jr., "Two- and Three-Dimensional Neutronics Calculations for the TFTR Neutral Beam Injectors," ORNL/TM-6354, Oak Ridge National Laboratory (1978), accepted for publication in Nuclear Science and Engineering.
3. R. G. Alsmiller, Jr. J. Barish, R. T. Santoro, R. A. Lillie, J. M. Barnes and M. M. H. Ragheb, "Dose Rates From Induced Activity in the TFTR Test Cell," ORNL/TM-6904, Oak Ridge National Laboratory (in press), submitted to Nuclear Technology.
4. B. Pritchard, Princeton Plasma Physics Laboratory, private communication.
5. W. A. Rhoades and F. R. Mynatt, "The DOT III Two-Dimensional Discrete Ordinates Code," ORNL/TM-4280, Oak Ridge National Laboratory (1973).
6. M. B. Emmett, C. E. Burgart, T. J. Hoffman, "DOMINO, A General Purpose Code for Coupling Discrete Ordinates and Monte Carlo Radiation Transport Calculations," ORNL-4853, Oak Ridge National Laboratory (1973).
7. M. B. Emmett, "The MORSE Monte Carlo Radiation Transport System," ORNL-4972, Oak Ridge National Laboratory (1975).
8. R. L. Childs, Oak Ridge National Laboratory, private communication.
9. ORNL/RSIC-37, Radiation Shielding Information Center, Oak Ridge National Laboratory (1975), also available as DLC-41/VITAMIN C.

References(Cont'd)

10. NCRP Report No. 38, Protection Against Neutron Radiation, National Council on Radiation Protection and Measurements (1971).

11. H. C. Claiborne and D. K. Trubey, Nucl. Tech. 450 (1970).

ACKNOWLEDGEMENTS

The authors wish to thank G. Sheffield, R. Little, K. Young, H. J. Howe, Jr. and Long-Poe Ku of the Princeton Plasma Physics Laboratory for their comments and guidance throughout this study.

ORNL/TM-6949
Dist. Category UC-20d
(Fusion Systems)

Internal Distribution

1. L. S. Abbott
2. F. S. Alsmiller
3-7. R. G. Alsmiller, Jr.
8. J. Barish
9-13. J. M. Barnes
14. D. E. Bartine
15. L. A. Berry
16. G. F. Flanagan
17. T. A. Gabriel
18. H. Goldstein (Consultant)
19-23. R. A. Lillie
24. F. C. Maienschein
25. R. W. Peelle
26. RSIC
27-36. R. T. Santoro
37. D. Steiner
38. P. Greebler (Consultant)
39. W. B. Loewenstein (Consultant)
40. R. E. Uhrig (Consultant)
41. R. Wilson (Consultant)
42-43. Central Research Library
44. ORNL Y-12 Technical Library
Document Reference Section
45. Laboratory Records Department
46. ORNL Patent Office
47. Laboratory Records - RC

External Distribution

48. F. E. Coffman, Chief, Systems and Applications Studies Branch, Office of Fusion Energy, Department of Energy, Washington, D.C. 20545
49. W. Cooper, Lawrence Berkeley Laboratory, Neutral Beam Group, Berkeley, CA 94720
50. J. N. Grace, Office of Fusion Energy, Department of Energy, Washington, D.C. 20545
51. C. R. Head, Office of Fusion Energy, G-234, Department of Energy, Washington, D.C. 20545
52. H. W. Hendel, Plasma Physics Laboratory, Princeton University, P. O. Box 451, Princeton, NJ 08540
53. R. Hensler, Ebasco Services, Inc., 2 Rector St., NY, NY 10006
54. H. J. Howe, Jr., Plasma Physics Laboratory, Princeton University, P.O. Box 451, Princeton, NJ 08540
55. R. Little, Plasma Physics Laboratory, Princeton University, P.O. Box 451, Princeton, NJ 08540
56. K. G. Moses, Office of Fusion Energy, Department of Energy, Washington, D.C. 20545
57. L. C. Pittenger, Lawrence Livermore Laboratory, P.O. Box 808, L-383, Livermore, CA 94550
58. L. K. Price, Office of Fusion Energy, Department of Energy, Washington, D.C. 20545
59. B. Pritchard, Plasma Physics Laboratory, Princeton University, P.O. Box 451, Princeton, NJ 08540
60. P. J. Reardon, Plasma Physics Laboratory, Princeton University, P.O. Box 451, Princeton, NJ 08540

External Distribution (Cont'd)

61. Yasushi Seki, Japan Atomic Energy Research Institute, Tokai-mura, Ibaraki-ken, Japan
62. G. Sheffield, Plasma Physics Laboratory, Princeton University, P.O. Box 451, Princeton, NJ 08540
63. E. Stern, Plasma Physics Laboratory, Princeton University, P.O. Box 451, Princeton, NJ 08540
64. K. Wright, Plasma Physics Laboratory, Princeton University, P. O. Box 451, Princeton, NJ 08540
65. K. Young, Plasma Physics Laboratory, Princeton University, P.O. Box 451, Princeton, NJ 08540
66. Office of Assistant Manager, Energy Research and Development, DOE-ORO, Oak Ridge, Tennessee 37830

67-217. Given distribution as shown in TID-4500, Magnetic Fusion Energy (Distribution Category UC-20d: Fusion Systems)